AIAA 80-1037R

Structure-Borne Noise Prediction for a Single-Engine General Aviation Aircraft

J. F. Unruh*
Southwest Research Institute, San Antonio, Texas

The usefulness of a deterministic modeling procedure employing structural-acoustic finite-element formulations is investigated for the prediction of structure-borne interior noise. Analytical predictions are compared to normal mode, forced harmonic response, and engine-running experimental data obtained during ground tests of a single-engine general aviation aircraft. From these comparisons, the modeling procedures are shown to be sufficiently accurate for structure-borne interior noise prediction.

Nomenclature

A	= subscript denoting acoustic region
B	= a product of two matrices defined in Eq. (3)
$C_A(\omega)$	= acoustic damping matrix, frequency dependent
C_S	= structural damping matrix
F	= externally applied structural forces
$\bar{F}$	= generalized applied forces
I	= subscript or superscript denoting interior region and unit diagonal matrix
K	= stiffness matrix, in general
M	= mass matrix, in general
P	= nodal perturbation pressure, in general
q_A	= acoustic subvolume modal degrees of freedom
q_S	= structural modal degrees of freedom
Q	= eigenvectors, in general
r	= subscript denoting rth coupled mode
S	= surface of acoustic region; also subscript or superscript denoting surface nodes
T	= decoupling transformation submatrix
u	= structural nodal displacements
W	= transformed mass matrix
β	= critical damping ratio
γ	= coupled system modal degrees of freedom
Ψ	= coupled system eigenvectors
ω	= circular frequency

Introduction

A RECENT experimental study[1] has shown that engine-induced structure-borne noise can be the primary source of interior noise in single-engine general aviation aircraft. Nonweighted interior noise spectra were shown to be dominated by low-frequency responses below 100 Hz; and a shift in peak response to the higher frequency region, around 1000 Hz, occurred when A-weighted corrections were applied. However, the relative importance of the higher frequency response in the A-weighted spectra were shown to diminish with increased engine rpm due to increased response at the propeller tone. From this study, it was concluded that if substantial overall noise reduction were to be achieved, structure-borne noise control measures applicable to the lower frequency region must be developed.

To reduce structure-borne interior noise at the airframe design stage will require adequate prediction procedures; however, the propagation and radiation of structure-borne interior noise is a difficult process to analyze in exact form.[2] Nevertheless, recent developments[3-5] in coupled structural-acoustic analysis techniques have formulated more deterministic modeling procedures for structure-borne interior noise prediction. In the present investigation, the subvolume analysis technique described in Ref. 5 is used for structure-borne interior noise prediction in a single-engine general aviation aircraft. Predicted fuselage structural and interior acoustic normal modes are compared to measured responses in a typical general aviation aircraft fuselage. Predicted single-axis forced harmonic fuselage acceleration and cabin sound pressure level responses are compared directly to laboratory-measured transfer function data. Recorded engine excitation forces are also applied to the coupled structural-acoustic model and comparisons are made to interior noise levels recorded during engine-running ground tests.

In the sections to follow, a brief review of the method of analysis as detailed in Refs. 1 and 5 is given along with a description of the fuselage structural and interior acoustic finite-element models used in the study. Thereafter, numerical results obtained with the models are compared to various experimental results to demonstrate the usefulness of the analysis method. A limited discussion on structure-borne noise control measures in the low-frequency region is also presented.

Method of Analysis

Finite-element structural and acoustic representations of a flexible structure and receiving acoustic volume are used to formulate the equations of motion for the coupled structural-acoustic system. The matrix structural equations of motion take the form

$$[M_S]\{\ddot{u}\} + [C_S]\{\dot{u}\} + [K_S]\{u\} = [K_{SA}]\{P_S\} + \{F\} \quad (1)$$

where M_S, C_S, and K_S are, respectively, the assembled nodal mass, damping, and stiffness matrices for the structure and u the nodal degrees of freedom. The applied loads are due to the acoustic back pressure associated with the nodal surface pressures P_S and the externally applied forces to the structure F.

Likewise, the assembled matrix form of the acoustic equations of motion is

$$\left[\begin{array}{c|c} M_A^{SS} & M_A^{SI} \\ \hline M_A^{IS} & M_A^{II} \end{array}\right] \left\{\begin{array}{c} \ddot{P}_S \\ \hline \ddot{P}_I \end{array}\right\} + \left[\begin{array}{c|c} C_A(\omega) & 0 \\ \hline 0 & 0 \end{array}\right] \left\{\begin{array}{c} \dot{P}_S \\ \hline \dot{P}_I \end{array}\right\}$$

$$+ \left[\begin{array}{c|c} K_A^{SS} & K_A^{SI} \\ \hline K_A^{IS} & K_A^{II} \end{array}\right] \left\{\begin{array}{c} P_S \\ \hline P_I \end{array}\right\} = \left[\begin{array}{c} -M_{AS} \\ \hline 0 \end{array}\right] \{\ddot{u}\} \quad (2)$$

where M_A, $C_A(\omega)$, and K_A are the acoustic nodal mass, damping, and stiffness matrices, respectively, and M_{AS} the inertia coupling associated with the boundary motion. The pressure nodal degrees of freedom are partitioned into those

Presented as Paper 80-1037 at the AIAA 6th Aeroacoustics Conference, Hartford, Conn., June 4-6, 1980; submitted July 24, 1980; revision received Dec. 22, 1980.

*Senior Research Engineer, Department of Mechanical Sciences. Member AIAA.

nodes on the surface P_S wherein damping or boundary motion is present and all other degrees of freedom are referred to as interior nodes P_I.

Modal expansion and truncation techniques[1,5] are first used to reduce the number of structural (u) and interior pressure (P_I) degrees of freedom to modal form q_s and q_A, respectively. The symmetric form of the resulting quasimodal equations is

$$\begin{bmatrix} \ddots\omega_S^2\ddots & 0 & 0 \\ 0 & W_A^{SS} & W_A^{SI}Q_A \\ 0 & Q_A^T W_A^{IS} & \ddots I \ddots \end{bmatrix} \begin{Bmatrix} \ddot{q}_S \\ \ddot{P}_S \\ \ddot{q}_A \end{Bmatrix} + \begin{bmatrix} \ddots 2\beta_S\omega_S^3 \ddots & 0 & 0 \\ -B^T[\ddots 2\beta_S\omega_S^2 \ddots] & C_A(\omega) & 0 \\ 0 & 0 & 0 \end{bmatrix} \begin{Bmatrix} \dot{q}_S \\ \dot{P}_S \\ \dot{q}_A \end{Bmatrix} + \begin{bmatrix} \ddots \omega_S^4 \ddots & -[\ddots\omega_S^2\ddots]B & 0 \\ -B^T[\ddots\omega_S^2\ddots] & S_A^{SS}+B^TB & 0 \\ 0 & 0 & \ddots\omega_A^2\ddots \end{bmatrix} \begin{Bmatrix} q_S \\ P_S \\ q_A \end{Bmatrix} = \begin{bmatrix} \ddots\omega_S^2\ddots \\ -B^T \\ 0 \end{bmatrix} \{Q_S^T F\} \tag{3}$$

where $B=Q_S^T K_{SA}$ and is referred to as the coupling matrix, and

$$W_A^{SS}=M_A^{SS}+T^TM_A^{IS}+M_A^{SI}T+T^TM_A^{II}T$$

$$W_A^{SI}=(W_A^{IS})^T=M_A^{SI}+T^TM_A^{II}$$

$$S_A^{SS}=K_A^{SS}=T^TK_A^{IS} \tag{4}$$

with

$$T=-[K_A^{II}]^{-1}[K_A^{IS}]$$

The nodal structural motions are related to the modal degrees of freedom via the eigenvectors Q_S as

$$\{u\}=[Q_S]\{q_S\} \tag{5}$$

and the interior nodal pressures are related to the nodal surface pressures and interior acoustic modal eigenvectors Q_A as

$$\{P_I\}=[T]\{P_S\}+[Q_A]\{q_A\} \tag{6}$$

For the case where the acoustic absorptive terms $C_A(\omega)$ in Eq. (3) may be considered constant, i.e., not a function of frequency, we may expand the damped nonhomogeneous equations in terms of the undamped homogeneous coupled structural-acoustic modes. This results in

$$[\ddots I \ddots]\{\ddot{\gamma}\}+[C_{SA}]\{\dot{\gamma}\}+[\ddots\omega_{SA}^2\ddots]\{\gamma\}=\{\bar{F}\} \tag{7}$$

where ω_{SA} are the coupled structural-acoustic normal mode frequencies which correspond to the eigenvectors Ψ, defined as

$$\begin{Bmatrix} q_S \\ P_S \\ q_A \end{Bmatrix} = [\Psi]\{\gamma\} \tag{8}$$

The generalized forces are defined by

$$\{\bar{F}\}=[\Psi^T]\begin{bmatrix} \ddots\omega_S^2\ddots \\ B^T \\ 0 \end{bmatrix}\{Q_S^T F\} \tag{9}$$

The generalized damping matrix has the form

$$[C_{SA}]=[\Psi^T]\begin{bmatrix} \ddots 2\beta_S\omega_S^3 \ddots & 0 \\ -B^T[\ddots 2\beta_S\omega_S \ddots] & C_A \end{bmatrix}[\Psi] \tag{10}$$

where it can be seen that when there is no acoustic absorption ($C_A=0$), there still exists a damping coupling between the structural and acoustic degrees of freedom. In the results to be presented in this investigation, it is assumed that the damping matrix is diagonalized by the coupled system eigenvectors such that

$$[C_{SA}]=[2\beta_{SA}\omega_{SA}] \tag{11}$$

where β_{SA} are the coupled mode critical damping ratios. This approximation has the computational advantage of completely diagonalizing the nonhomogeneous system of equations. The resulting solution appears as a series of damped uncoupled single-degree-of-freedom oscillators. The solution of the rth coupled degree of freedom for a forced harmonic input is simply

$$\gamma_r=\frac{\bar{F}_r(\omega)}{(\omega^2_{SA}-\omega^2)+i2\beta\omega_{SA}\omega} \tag{12}$$

This approximate solution has been shown to be most appropriate for lightly damped systems[5,6], however, it requires knowledge of the *coupled mode* critical damping ratios.

Finite-Element Models

Structural Model

A structural finite-element model of the test aircraft fuselage was developed based on the structural data found in Ref. 7 and physical measurements taken directly from the aircraft. The primary aircraft carry-through structure is provided by a channel-stiffened double-skin floor and the forward and aft door frames. The fuselage primary structure is shown in Fig. 1. The skin thickness of the various fuselage panels varied 0.051-0.025 in. Due to the symmetry of the fuselage, a symmetric half-plane model was developed. The fuselage was modeled using 165 three-dimensional beam elements for the primary fuselage structure and 200 shell elements for the various fuselage skin panels. Lumped masses were employed to represent mass loading from various nonstructural fuselage members. Included were such items as the battery, fuel system, rudder controls, instrumentation, landing gear, etc.

Rather than attempt to model all localized plate motion, only those panel sections which were found to produce significant responses during modal sweep tests[1] were modeled in detail. The analysis range of primary interest in this initial investigation was just past the second propeller tone or out to approximately 150 Hz. In this frequency region, it was expected that the response would be dominated by motion of the tail cone side panels, fuselage doors, cabin side windows, cabin roof, and rear cabin side panels. The finite-element model was generated using the EASE2[8] structural analysis program and consisted of 767 dynamic degrees of freedom. The resulting finite-element model is shown in Fig. 2.

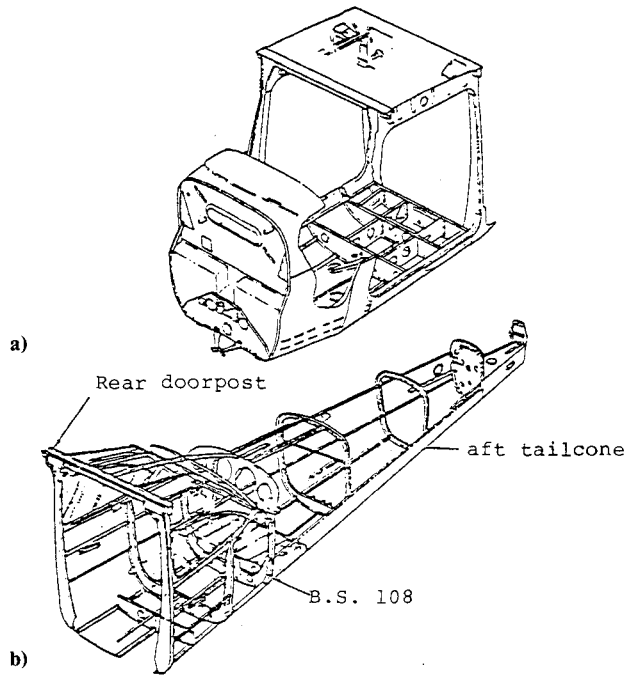

Fig. 1 Fuselage primary structure. a) Front and center section assembly. b) Aft cabin and tail cone assembly.

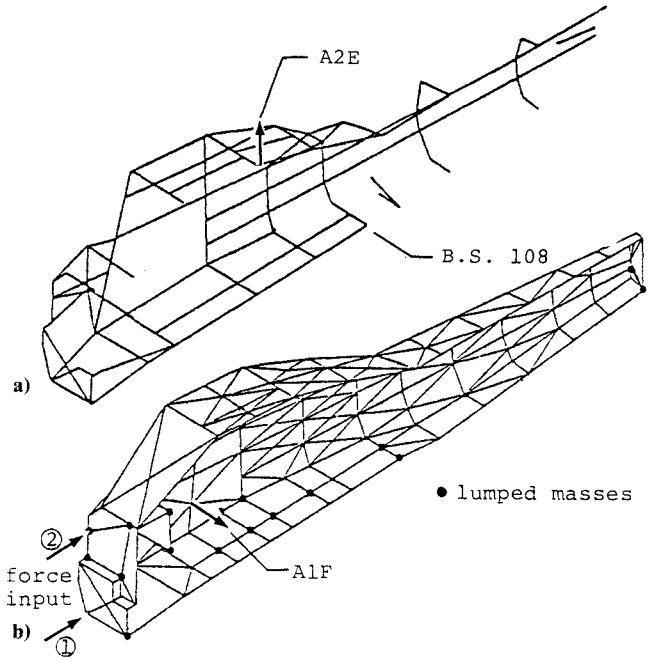

Fig. 2 Fuselage structural finite-element model. a) Beam elements. b) Beam and shell elements.

Interior Acoustic Model

Two finite-element acoustic models of the fuselage interior were developed: a full-fuselage model which physically occupied the volume prescribed by the structural symmetric half-plane model; and a cabin-only model which considered the interior bulkhead at body station 108 to be rigid, thereby terminating at that point. Many of the surface acoustic node points were coincident with the structural nodes. The basic division of acoustic nodes followed the structural model shown in Fig. 2. In Fig. 3, the distribution of acoustic node points at major fuselage stations is given to indicate the density of acoustic interior node points within the fuselage. The full-fuselage acoustic model consisted of a total of 124 surface nodes P_S and 74 interior nodes P_I throughout the

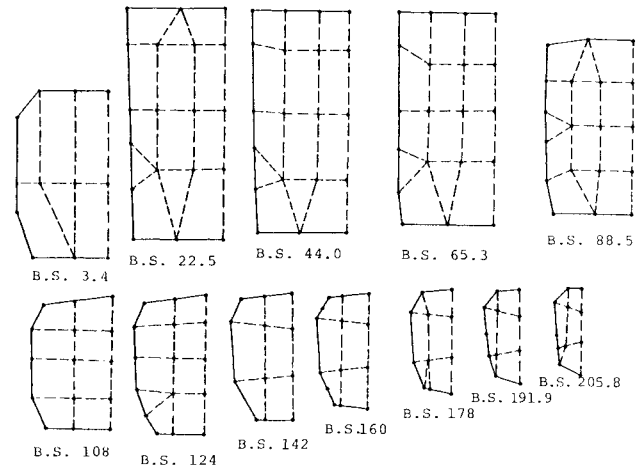

Fig. 3 Distribution of acoustic node points at major fuselage stations.

half-plane model. In full-fuselage model, 90 of the surface nodes were considered elastically active; the remaining 108 nodes were considered stationary. The model had a total of 98.6 ft^2 of surface area of which approximately 64% was considered active in the coupled-fuselage model. In the cabin-only model, 61 of the 124 nodes were active surface nodes representing 46.1 ft^2 of surface area. The full-fuselage model required a total of 124 three-dimensional acoustic volume elements to form the model acoustic mass and stiffness matrices and 106 surface interaction elements to form the surface coupling matrix K_{SA}. The cabin-only model required 80 acoustic volume elements and 77 surface interaction elements.

The maximum width of the fuselage was 42 in., which prevented antisymmetric acoustic response below 160 Hz. Thus, there was no need to compute antisymmetric fuselage motions for the desired modeling range.

The analysis software used to develop the acoustic models and carry out the structural-acoustic coupling and solution procedures was developed at Southwest Research Institute using FORTRAN IV on a CDC 6600 computer. The software was limited in representation to 150 dynamic degrees of freedom for the acoustic model and overall coupled-model representations. Through the use of an acoustic subvolume analysis technique,[5] the software could, however, accommodate a total of 200 acoustic modal degrees of freedom and 32 structural modal degrees of freedom. Due to this software limitation, a majority of the model comparisons discussed in the following section employed the somewhat smaller cabin-only acoustic model.

Comparison of Results

Normal Mode Frequencies

A summary of experimental and predicted normal mode frequencies for the fuselage structure and interior acoustic volume are given in Table 1. Interior acoustic resonances were experimentally determined for three configurations: 1) a standard cabin interior wherein a highly flexible bulkhead at body station 108 divided the cabin area from the fuselage tail cone; 2) cabin-only, wherein a rigid partition replaced the bulkhead at station 108; and 3) a full-fuselage, wherein the bulkhead at station 108 was completely removed. Acoustic hard-walled modes were computed for both the cabin-only and full-fuselage acoustic models. The fundamental cabin-only hard-walled mode was predicted at 71.6 Hz compared to 62.0 Hz measured in the laboratory. Likewise, hard-walled full-fuselage fundamental responses were predicted to be 40.0 and 72.7 Hz, while the laboratory results showed responses at 34.0 and 63.0 Hz, respectively. Predicted fuselage midplane node line plots are given in Fig. 4 for the acoustic hard-walled modes below 100 Hz.

Table 1 Summary of normal mode frequencies, Hz

	Experimental			Predicted					
	Acoustic				Acoustic hard walled			Coupled responses	
Mode No.	Standard cabin	Cabin only[a]	Full fuselage[b]	Structural	Cabin	Fuselage	Structure alone, SA	Cabin plus structure, CC	Fuselage plus structure, CF
1	32.6	62.0	34.0	30.0	71.6	40.0	26.61	28.04	25.40
2	40.4		63.0	44.0	131.5	72.7	39.26	39.25	31.61[d]
3	61.9			44.0	160.5	104.1	41.95	41.94	40.07
4				45.0	188.0	138.0	42.16	42.46	42.89
5				56.4	222.8	159.0	56.38	56.37	52.13
6				60.0	234.5	179.5	61.52	57.91	56.76
7				(63)[c]	284.2	197.2	67.86	66.01[d]	60.67
8				73.0	304.9	229.9	72.92	68.27	67.48
9				73.0	327.3	236.0	75.98	73.44	68.94[d]
10				80.0			81.37	77.01	73.22
11				(80)			82.52	80.67	77.04
12				(100)			95.40	83.84	79.93
13				(90)			100.46	96.42	83.79
14				–			103.91	100.69	96.46
15				98.0			107.65	103.41	99.86

[a] Bulkhead at body station 108 rigid. [b] Bulkhead at body station 108 removed. [c] Response taken from one-third octave acceleration data. [d] Primarily acoustic response.

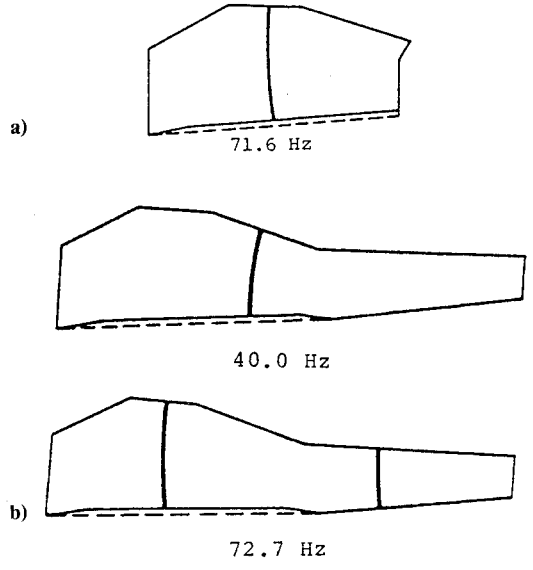

Fig. 4 Predicted acoustic hard-walled modes below 100 Hz. a) Cabin only. b) Full fuselage.

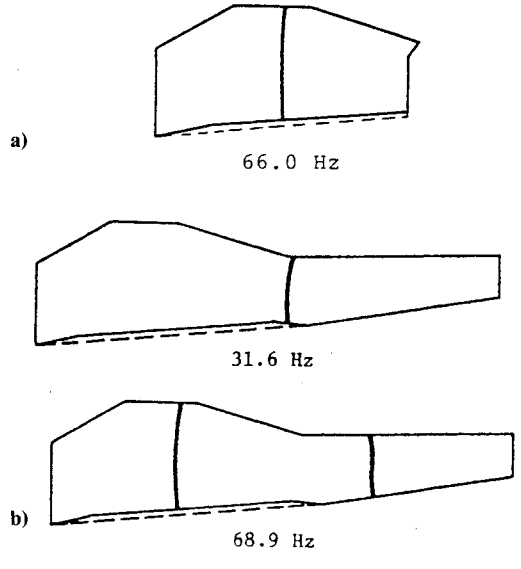

Fig. 5 Predicted primarily acoustic coupled normal mode responses below 100 Hz. a) Cabin only. b) Full fuselage.

Measured critical damping ratios for the acoustic responses ranged 0.016-0.030, except for the 32.6 Hz standard cabin fundamental mode wherein a damping ratio of 0.054 was measured. This relatively high damping value was attributed to flow leakage and structural damping via volume pumping between the fuselage cabin and the tail cone volumes across the flexible bulkhead at body station 108. Damping for all other modes is attributed to coupling to the structure; appreciable acoustic absorption from the interior trim at these low frequencies is very unlikely.

Thirty-six elastic modes were retained from an eigenvalue analysis of the fuselage finite-element structural model. The aircraft rigid-body support frequencies were sufficiently low (below 11 Hz) such that they were decoupled from the aircraft elastic response and, therefore, they were not retained in the model. A comparison of the resulting modal frequencies and experimentally determined frequencies is also given in Table 1. As can be seen, the predicted frequencies are in quite good agreement with the measured responses. The primary fuselage vertical bending modes were predicted to be at 56.4 and 119 Hz. The first vertical bending response precisely agreed with the measured response. Panel responses up through 100 Hz also compare well with the measured values.

The structural modal density of the aircraft for the modeled range, up to 150 Hz, was computed to be on the order of 0.3 mode/Hz. The high structural modal density of the fuselage limited representation to 32 elastic modes, or an upper frequency range of 200 Hz. While modes up to 200 Hz are included in the analysis, it is to be noted that some lack of representation exists in the frequency range above 150 Hz.

The effect of wall flexibility on the predicted normal mode responses can be seen in Table 1 by comparison of the hard-wall frequencies to the coupled structural-acoustic frequencies. All of the computed coupled normal mode responses exhibit structural-acoustic coupling to some degree. However, by examination of the midplane node line plots, as given in Fig. 5, we can see that the fundamental acoustic cabin resonances dropped from 71.6 Hz in the hard-walled model to 66.0 Hz in the coupled model. Likewise, in the full-fuselage coupled model predictions, the fundamental acoustic normal

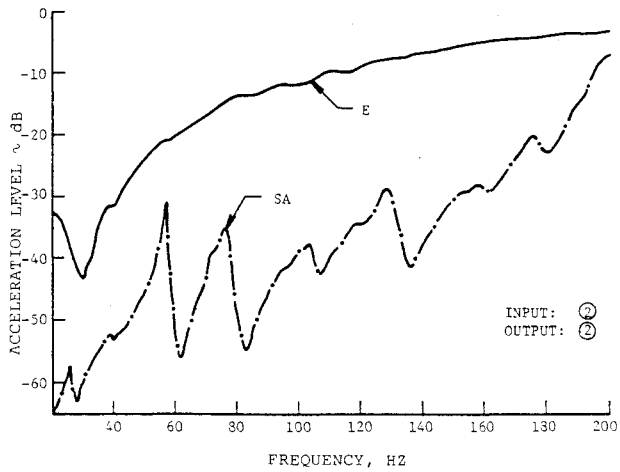

Fig. 6 Driving point acceleration response for longitudinal harmonic input of 44.48 N rms.

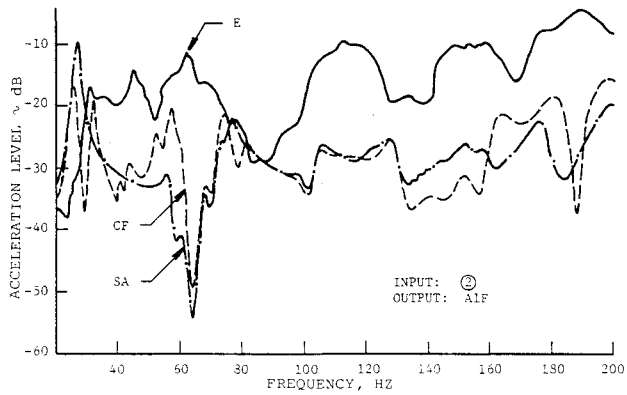

Fig. 7 Lateral acceleration response at AIF for longitudinal harmonic input of 44.48 N rms.

mode responses dropped from 40.0 and 72.7 Hz to 31.5 and 68.9 Hz when wall flexibility was taken into account. Comparisons of the coupled normal mode predictions to the measured responses clearly show that including wall flexibility has greatly improved agreement between predicted and measured results. It is to be noted that each of the coupled acoustic normal modes, even though primarily a structural response, have well-defined acoustic nodal patterns within the cabin. The coupled mode node line plots given in Fig. 5 were selected to correspond to their hard-walled counterparts given in Fig. 4.

Transfer Functions

Forced harmonic sweep data were recorded in the laboratory by exciting the fuselage at the engine attach points with an electrodynamic shaker. Structural responses were recorded at various frame and panel members, and interior sound pressure levels were recorded at various interior locations while maintaining a constant input force. The analytical model was exercised to simulate the various test conditions. A comparison of typical results are shown in Figs. 6-9. For a majority of these cases, the input force was at the engine mount upper attach point in the longitudinal direction. Reference is made to Fig. 2 for the various input and response locations presented in this study. The analyses were carried out using the expression given in Eq. (12), wherein a coupled-mode critical damping ratio of $\beta_{SA} = 0.02$ was used for all modes. The pressure, acceleration, and force level data presented in the following discussions are computed as 20 $\log_{10}$ (rms level/reference) where the reference values are 2.0×10^{-5} N/m^2, 1.0 g, and 88.96 N, respectively. The various data curves are keyed by experimental results (E),

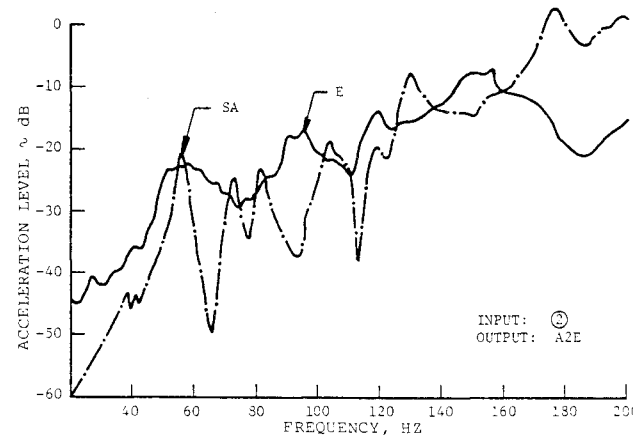

Fig. 8 Vertical acceleration response at A2E for longitudinal harmonic input of 44.48 N rms.

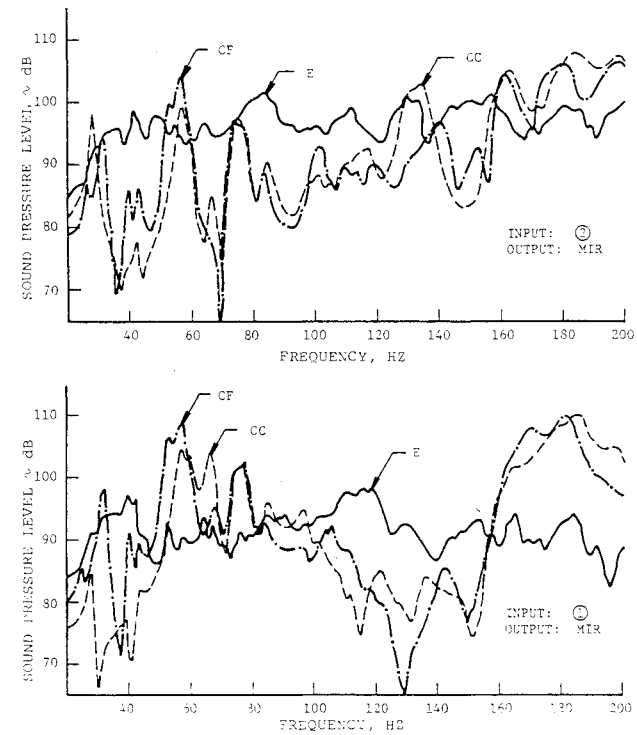

Fig. 9 Sound pressure level at MIR for longitudinal harmonic input of 44.48 N rms.

structure alone model predictions (SA), cabin only model predictions (CC), and full-fuselage model predictions (CF).

In Fig. 6, the acceleration response of the structural model alone is compared to the measured response at the driving point. As can be seen, the analytical model is considerably stiffer in this local region than the actual fuselage. This is not surprising when considering the finite-element density in this area (see Fig. 2). However, the computed acceleration response on a lower door panel, as given in Fig. 7, shows improved agreement when compared to the measured response. It was found that reasonably good correlation of acceleration responses occurred on most major frame members. Typical results are shown in Fig. 8 for the acceleration response at the top center of the rear door frame.

During the sweep tests, interior sound pressure level (SPL) responses were recorded at several locations near the pilot's normal head position, denoted as MIR. At any one microphone, large variations in the SPL spectrum occurred due to a high number of panel and acoustic resonant responses within the cabin. These large variations were smoothed by enveloping the spectra from several of the

microphones near MIR. Similar envelopes were developed with the analytical model predictions. Both the full-fuselage and the cabin-only coupled acoustic models were exercised and results compared to laboratory data. In Fig. 9a, a comparison of data is given for force excitation in the longitudinal direction at the upper engine attach point. The predicted results for the two acoustic models are in close agreement; however, the predictions are not conservative with respect to the measured results. The SPL spectra shown in Fig. 9b are results for a longitudinal input at the lower engine attach point. For this case, we see that the predictions are conservative in a portion of the spectrum. In general, the variation in SPL correlated well with the variations in panel acceleration response, as should be expected.

It is of interest to note that the response near 56 Hz, flagged with the CF label in both Figs. 9a and 9b, is primarily a response due to the fuselage vertical bending mode, reference 56.4 Hz. A high interior acoustic response was not noted for the fundamental fuselage mode during the mode searches. It is felt that this high response was due to the lack of complete panel representation in the cabin area. Recall that in the analytical model, only 64% of the total fuselage panel area was considered dynamically active. Due to this lack of representation, proper cancellations of panel sources throughout the cabin may not have occurred, thereby giving rise to a substantial net source. Other peak responses in the spectra are easily identified as fundamental acoustic and/or panel resonant responses.

From the system resonant frequency and transfer function data comparisons, it was concluded that the modeling procedures employed were correct and to improve the correspondence between measured and predicted results would require increasing both the structural definition of the fuselage and increasing the acoustic definition of the interior volume. Nevertheless, it was felt that the degree of correlation obtained with the present model was sufficient to allow further comparisons using measured engine input forces.

Engine Excitation

Engine-running ground tests were carried out on the aircraft to determine the contribution of engine-induced structural-borne noise to recorded interior SPL.[9] The engine-alone contribution was determined from mean one-third octave interior spectra taken from multiple engine attached and detached runs. During these runs, strain levels in the engine mounts were recorded and from these data the dynamic engine input forces were determined. The symmetric contribution of the engine input forces for an engine speed of 1920 rpm are given in Fig. 10. As can be seen, the input forces are a set of discrete tones at each engine ½ rpm harmonic. These input forces were applied individually to the cabin-only coupled model and interior SPL responses were computed. The total interior response was then computed using a square root of the sum of the squares method to account for the lack of relative phase information between the input forces.

A comparison of predicted and experimental one-third octave interior SPL at MIR is given in Fig. 11. The experimental data in Fig. 11 are indicated by the bar levels and the predicted results by the indicated symbols. Recall that the fundamental cabin acoustic resonance occurred at 64 Hz, which lies directly on an engine ½ rpm harmonic. This accounts for the high response in the test data in the 63 Hz band. When attempting to predict this response, it was necessary to increase the engine rpm from 1920 to 1980 since the cabin resonance occurred in the analytical model at 66 Hz. Predictions were made at two levels of damping, $\beta_{SA} = 0.01$ and 0.02. A factor of two increase in modal damping results in a 6 dB decrease in response at the cabin resonance. As expected, off-resonance response is not greatly affected by application of damping. The relatively low predicted response in the 31.5 Hz band in Fig. 11 reflects the cabin-only model geometry which does not support the full-fuselage fundamental cabin mode. However, the predicted results compare well to the interior-installed test data due to the presence of the bulkhead at body station 108 which resulted in suppressing the low-frequency mode. When the interior was removed, the 34 Hz mode was highly excited.

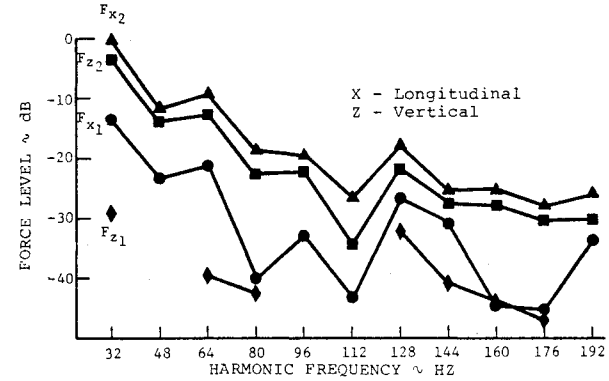

Fig. 10 Engine symmetric excitation forces, 1920 rpm.

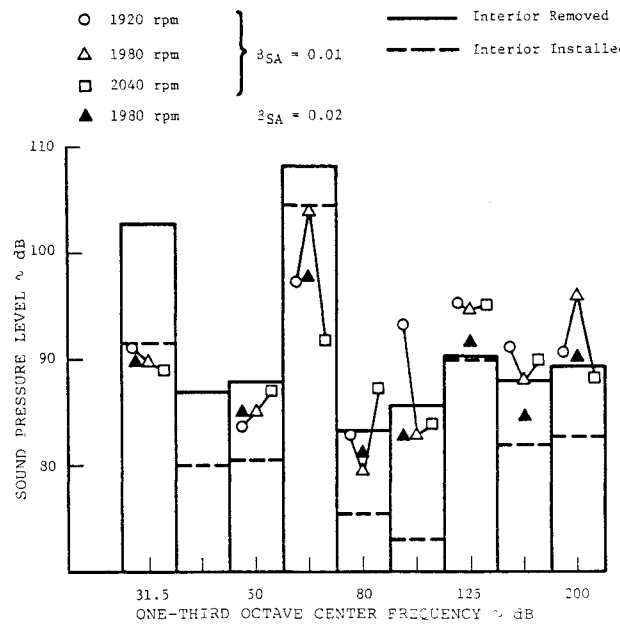

Fig. 11 One-third octave SPL at MIR, effect of cabin resonance.

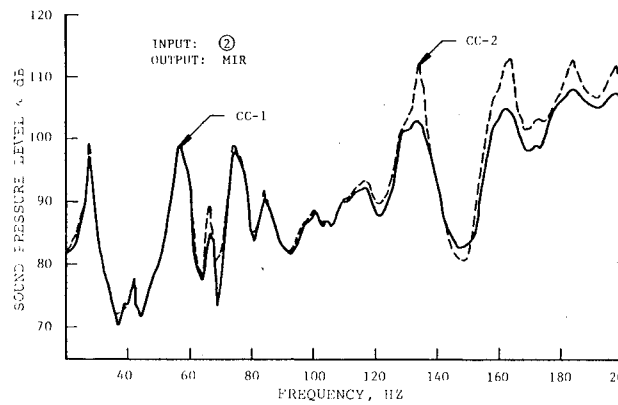

Fig. 12 Sound pressure level response at MIR, effect of damping representation.

Noise Control Measures

Only a limited investigation of noise control measures for this aircraft was carried out during this preliminary investigation. We have shown that increased damping is a viable

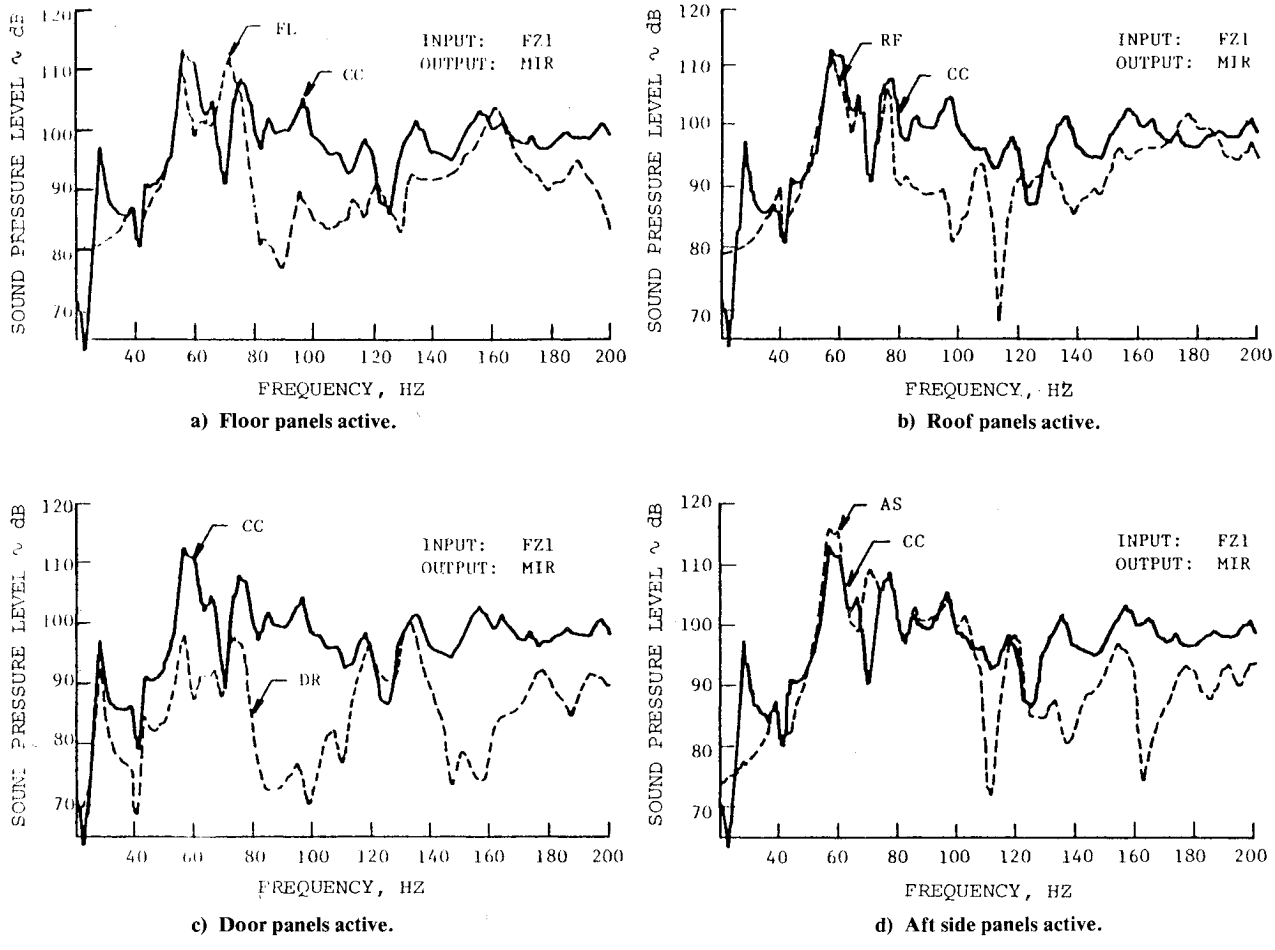

a) Floor panels active.

b) Roof panels active.

c) Door panels active.

d) Aft side panels active.

Fig. 13 Effect of panel groups on response at MIR for vertical harmonic input of 44.48 N rms.

control measure at highly resonant conditions. It is of interest to note that if only structural damping were input into the model, then only through structural-acoustic coupling would the acoustic response be damped. This is seen by the data given in Fig. 12 wherein predicted results for the SPL responses at MIR are given for two cases: case 1, flagged CC-1, represents the Eq. (11) approximation where all coupled modes are assigned $\beta_{SA} = 0.02$; and case 2, flagged CC-2, are results generated from employing Eq. (10) with damping ratios of $\beta_S = 0.02$ applied only to the structural modes. From these data, the primarily acoustic resonant responses are easily recognized by their increased amplitudes for the CC-2 damping representation. It is also apparent from these data that as the structural-acoustic coupling diminishes, as in the higher frequency region, the need to include acoustic absorption becomes more important to control acoustic resonant response.

The cabin-only model was used to investigate the sensitivity of interior noise levels to various panel groups in the aircraft. In this investigation, it was assumed that the structural compliance of the fuselage remained unchanged while various panel sections were individually activated. Mathematically, this required altering the coupling matrix B [reference Eq. (3)] to allow coupling motion only for the active panel group of interest; effectively all other panels were then rigid. Four panel groups were considered in the investigation: floor (11.2 ft^2), roof (11.0 ft^2), door (12.4 ft^2), and aft side (11.5 ft^2) panels. Separate coupled cabin models were generated with the four panel groups individually active. The effect of each of the panel groups on the sound pressure level near MIR for a constant force excitation in the vertical direction at the lower engine mount attach point is shown in Fig. 13. The response for all panels active is flagged as CC, where FL, RF, DR, and AS denote, respectively, floor, roof, door, and aft side panels. Upon inspection of these data, it can be seen that in certain frequency regions, several of the panel groups produce higher interior responses acting alone than when all groups act collectively. This is most pronounced for the floor panel and aft side panel responses given in Figs. 13a and 13d. From these data, we also note that for the given input, the door panels appear to be the least active group, while overall the aft side panels appear to be the most active group in generation of interior noise at MIR.

While it appears that at any fixed engine rpm, one panel group may respond more than other panel groups, it must be realized that the aircraft will operate over a rather broad rpm range. In flight, the test aircraft engine rpm can range 2100-2700 rpm. Thus, overall broadband response must be considered. For example, during flight operation, the propeller tone can vary 70-90 Hz. With a number of system resonances within this range, the individual responses can be controlled by application of damping material to the appropriate panel groups. Changes to the fuselage structural mass or stiffness properties can also remove panel resonances from highly excited frequency bands. However, no studies have been made to date to determine the tradeoffs between damping addition and structural changes. One structure-borne noise control measure that appears to be most appropriate would be to directly reduce the engine input excitation level by improved engine mount vibration isolation design.

Conclusion

Analytical finite-element coupled models of a test aircraft structure and acoustic volumes were developed for the purpose of determining modeling requirements for the prediction of structure-borne noise in lightweight single-engine aircraft structures. Comparison of predicted results to laboratory-measured aircraft response and to engine-running data has shown the analytical model to be reasonably accurate in the modeled frequency range. However, increased element

definition and the incorporation of acoustic absorption will be necessary to extend the model's useful frequency range.

From this preliminary investigation, several conclusions can be drawn:

1) Structural acoustic coupling can have a strong influence on fundamental cabin acoustic resonances in lightweight structures typical of single-engine general aviation aircraft.

2) Effective application of damping material to the structure will be limited to regions where panel resonant response predominates and will require strong structural-acoustic coupling to damp acoustic resonances.

3) Reduction of engine excitation transmission into the fuselage would appear to be the most viable low-frequency structural-borne noise control measure.

4) High modal densities of the aircraft fuselage and acoustic volume may limit the useful range of deterministic modeling procedures.

Acknowledgment

This work was conducted at Southwest Research Institute under contract to NASA Langley Research Center, Contract NAS1-14861.

References

[1] Unruh, J.F., Scheidt, D.C., and Pomerening, D.J., "Engine Induced Structural-Borne Noise in a General Aviation Aircraft," NASA Contractor Rept. 159099, Aug. 1979.

[2] Cremer, L., Hechl, M., and Ungar, E.E., *Structure-Borne Sound,* Springer-Verlag, New York, 1973.

[3] Craggs, A., "An Acoustic Finite Element Approach for Studying Boundary Flexibility and Sound Transmission Between Irregular Enclosures," *Journal of Sound and Vibration,* Vol. 30, No. 3, 1973, pp. 343-357.

[4] Dowell, E.H., Gorman, G.F. II, and Smith, D.A., "Acoustic-Elasticity General Theory, Acoustic Natural Modes and Forced Response to Sinusoidal Excitation, Including Comparisons with Experiment," *Journal of Sound and Vibration,* Vol. 52, No. 4, 1977, pp. 519-542.

[5] Unruh, J.F., "A Finite Element Subvolume Technique for Structural-Borne Interior Noise Prediction," *Journal of Aircraft,* Vol. 17, June 1980, pp. 434-441.

[6] Dowell, E.H., "Reverberation Time, Absorption and Impedance," *Journal of American Acoustical Society,* Vol. 64, No. 1, July 1978, pp. 181-191.

[7] Wittlin, G., Gamm, M.A., and Lubarge, W.L., "Full-Scale Crash Test Experimental Verification of a Method of Analysis for General Aviation Airplane Structural Crashworthiness," FAA-RD-77-199, 1976.

[8] Engineering Analysis Corp., "EASE2-Static/Dynamic Structural Analysis System," accessed through McDonnell Douglas Automation Co., Huntington Beach, Calif., 1978.

[9] Unruh, J.F. and Schedit, D.C., "Engine Induced Structural-Borne Noise in a General Aviation Aircraft," *SAE Transactions,* Vol. 88, 1980, pp. 2171-2184.